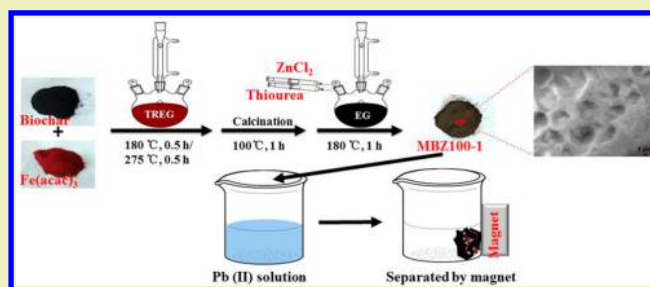


# Magnetic Biochar Decorated with ZnS Nanocrystals for Pb (II) Removal

Lili Yan,<sup>†,‡</sup> Long Kong,<sup>†</sup> Zan Qu,<sup>†</sup> Liang Li,<sup>\*,†</sup> and Guoqing Shen<sup>\*,‡</sup><sup>†</sup>School of Environmental Science and Engineering, Shanghai Jiao Tong University, 800 Dongchuan Road, Shanghai 200240, China<sup>‡</sup>School of Agriculture and Biology, Shanghai Jiao Tong University, 800 Dongchuan Road, Shanghai 200240, China

**ABSTRACT:** Magnetic biochar/ZnS composites were successfully synthesized by deposition of ZnS nanocrystals (NCs) on magnetic biochar in a polyol solution. The as-prepared composites showed a high maximum adsorption capacity for Pb (II) up to 367.65 mg g<sup>-1</sup>, which was 10 times higher than that of reported magnetic biochar. Furthermore, the lead-laden magnetic biochar/ZnS composites can be easily separated from the solution by a magnet after adsorption because of the excellent superparamagnetic properties. The composites were characterized by X-ray diffraction, scanning electron microscopy, and transmission electron microscopy. The adsorption process was well described by the pseudo-first-order model, and the adsorption isotherm could be well fitted by the Langmuir model. The thermodynamic studies showed that the removal of Pb (II) was an endothermic and spontaneous process. The present results warrant the promising application of magnetic biochar/ZnS composites in removal of Pb (II) from contaminated water.

**KEYWORDS:** ZnS, Wastewater, Magnetic, Biochar, Lead, Adsorption



## INTRODUCTION

The presence of lead (Pb) in aquatic ecosystems has become a great environmental concern worldwide. Due to its non-degradable property and tendency for bioaccumulation in the food chain, it poses a serious threat to human health, living organisms, and aquatic ecosystems, potentially effecting the entire ecosystem.<sup>1,2</sup> Therefore, much effort has been spent on removing Pb (II) in effluent wastewater. Traditional water treatment technologies, such as precipitation,<sup>3</sup> membrane separation,<sup>4</sup> adsorption,<sup>5</sup> flocculation,<sup>6</sup> and ion exchange<sup>7</sup> have been found to be effective in reducing Pb (II) concentration. Most of these technologies, however, may be associated with high operation cost and/or sludge disposal problems.

Biochar is a carbon-rich, low-cost, and solid byproduct of the thermal transformation of a biomass by pyrolysis under oxygen-limited conditions.<sup>8</sup> The porous structure and heterogeneous surface chemistry give biochar a strong sorption affinity to various metal ions. Biochar has attracted widespread attention for its potential use as a surface sorbent.<sup>9</sup> However, it is difficult to separate powdered biochar from the aqueous solution because of the small particle sizes.<sup>10</sup> It is an important goal for environmental scientists to establish a method of capturing contaminant metal ions in water with high efficiency and then to separate them out with ease.<sup>11</sup> In order to achieve this goal, recent research has been focused on preparing magnetic biochar materials by inducing magnetic nanoparticles into biochar. The introduction of a magnetic medium to the biochar allows lead to be completely separated from the solution by an external magnetic field.<sup>10–12</sup> However, the maximum adsorp-

tion capacity of a magnetic biochar composite for lead is relative low. This limits their practical application in wastewater treatment.

Nanomaterials are typically defined as materials smaller than 100 nm in at least one dimension.<sup>13</sup> They are excellent adsorbents, catalysts, and sensors due to their large specific surface area and high reactivity.<sup>14</sup> As a result of their innumerable unique properties, they have been explored for application in inorganic polluted water, dye wastewater, papermaking wastewater, pesticide wastewater, and oily wastewater treatment.<sup>15</sup> Typical representatives of this new material are semiconductor nanocrystals (NCs), known as quantum dots (QDs), nanomaterial made from a semiconductor nanostructure that confines the motion of conduction band electrons, valence band holes, and excitons in all three spatial directions.<sup>16,17</sup> NCs can become an ideal candidate for heavy metal removal applications. Pala<sup>18</sup> and Piquette<sup>19</sup> have reported removal of lead by using a ZnS nanomaterial. Jaiswal<sup>20</sup> showed that ZnS QDs-impregnated chitosan film could be used to remove heavy metal ions from contaminated water. Although NCs have a good adsorption ability, it is very difficult to separate and recycle the product from the aqueous solution because of their small sizes.

In this study, we reported a novel, highly efficient, magnetic biochar coated with ZnS nanocrystals (NCs) for removal of Pb (II) in water. Magnetic biochar/ZnS composites were

Received: September 29, 2014

Revised: November 4, 2014

Published: November 17, 2014

synthesized in a polyol solution and characterized. Adsorption kinetics and isotherms of Pb (II) on this innovative sorbent were investigated. The kinetic and equilibrium parameters were calculated. Then, the influence of pH on the adsorption was interpreted. Furthermore, the thermodynamic parameters were also determined.

## EXPERIMENTAL SECTION

**Materials.** Ethylene glycol (EG, >99%), triethylene glycol (TREG, >99%), 1-butylamine (>99%), zinc chloride (>99%), and lead nitrate (>99%) were provided by Aladdin Chemical (Shanghai, China). Ferric acetylacetonate ( $\text{Fe}(\text{acac})_3$ , 99%) was purchased from Energy Chemical (Shanghai, China). Thiourea (99%) was provided by Sinopharm Chemical Reagent Co., Ltd. Biochar was produced from rice hull through slow pyrolysis at 400 °C for 5 h in a ceramic fiber muffle furnace under an  $\text{O}_2$ -free atmosphere. The obtained biochar was ground to pass through a 0.125 mm sieve without further surface modification.

**Synthesis of Magnetic Biochar/ZnS Composites.** Biochar (500 mg) was added into 60 mL of TREG and sonicated for 5 min. Then, 1000 mg of the iron precursor  $\text{Fe}(\text{acac})_3$  was added under magnetic stirring. The resulting mixture was heated to 180 °C for 0.5 h, and then, under vigorous stirring and nitrogen protection, it was heated to reflux for 0.5 h (275 °C). After cooling to room temperature, the black mixture was washed with ethanol several times and dried in a vacuum overnight at 60 °C. The black product was labeled as MB, which was calcined at 100 °C in a tube furnace (BTF-1700C, AnHui BEQ Equipment Technology Co., Ltd., China) for 1 h to improve the crystal form and magnetism. The final product was marked as MB100.

A solution of MB100 (0.5 g) and EG (50 mL) was placed in a 100 mL three-necked flask equipped with a condenser. A zinc chloride EG solution (0.05 g  $\text{mL}^{-1}$ , 5 mL) and a mixture of 0.14 g of thiourea dissolved in 0.5 mL of 1-butylamine and 4.5 mL of EG were injected continuously and simultaneously into the reaction solution for 1 h by a syringe pump at 180 °C. The surface of the biochar is covered by hydroxyl groups,<sup>21</sup> which will adsorb  $\text{Zn}^{2+}$  that subsequently react with  $\text{S}^{2-}$  from decomposition of thiourea to form ZnS nanoparticles on magnetic biochar. Two magnetic biochar/ZnS composites were sampled from the reaction solution at 0.5 and 1 h, which were marked as MBZ100-0.5 and MBZ100-1, respectively.

**Characterization.** The X-ray diffraction (XRD) measurement was recorded on a Shimadzu XRD-6100. Scanning electron microscopy (SEM) images and energy dispersive X-ray (EDX) analysis of materials were taken with a JSM-7600F operated at 20 kV. The transmission electron microscopy (TEM) experiment was conducted on a JEM-2100F operated at 200 kV. The concentrations of Fe and Zn were determined by inductively coupled plasma atomic emission spectroscopy (ICP-AES, Varian 700-ES, U.S.A.). The magnetic measurement was carried out with a PPMS-9T (EC-II) of Quantum Design with a magnetic field up to 3 T.

**Absorption Experiments.** To perform adsorption kinetics analysis, a typical adsorption experiment was carried out by adding 20 mg of sorbent to 50 mL of Pb (II) solution (100  $\text{mg L}^{-1}$ ) in vials at 25 °C. At appropriate time intervals, aliquots were taken from the vials and immediately filtered through 0.22  $\mu\text{m}$  pore size membrane filters.

An adsorption isotherms experiment was carried out by mixing 60 mg of the sorbent with 50 mL of a Pb (II) solution at various concentrations in the range of 20–700  $\text{mg L}^{-1}$ . The vials were sealed and shaken in the mechanical shaker for 24 h to achieve the adsorption equilibrium state. Then, the mixtures were filtered. The amount of Pb (II) adsorbed by the sorbent at equilibrium ( $q_e$ ) was calculated using following equation

$$q_e = \frac{(C_0 - C_e)V}{m} \quad (1)$$

where  $C_0$  and  $C_e$  are initial and equilibrium concentrations of Pb (II) ( $\text{mg L}^{-1}$ ), respectively,  $V$  is volume of Pb (II) solution (L), and  $m$  is the mass of sorbent (g). The effects of pH on Pb (II) adsorption were

investigated at the pH values that were adjusted to 2.0, 3.0, 4.0, 5.0, and 6.0, with 0.1 M  $\text{HNO}_3$  and 0.1 M  $\text{NaOH}$ . To compare the removal efficiency of sorbents, 10 mg of biochar, MB100, or MBZ100-1 was added into 50 mL of a 100  $\text{mg L}^{-1}$  Pb (II) solution. The Pb (II) concentration in the filtrates was determined by atomic adsorption spectrometer (ControlAA 700, Analytik Jena AG, Germany).

## RESULTS AND DISCUSSION

**Characterization.** The structure and phase composition of MB, MB100, and magnetic biochar/ZnS composites are shown in the XRD patterns (Figure 1). The wide diffraction peak at

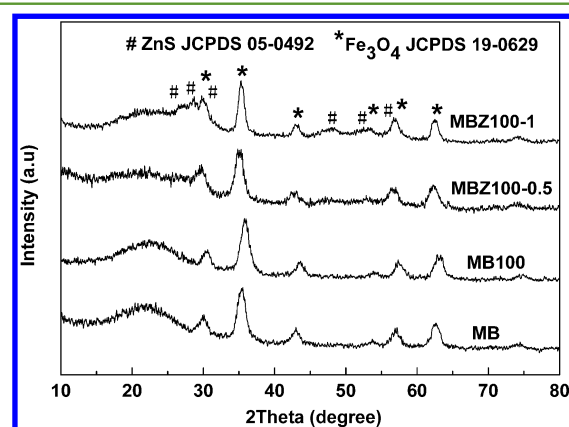
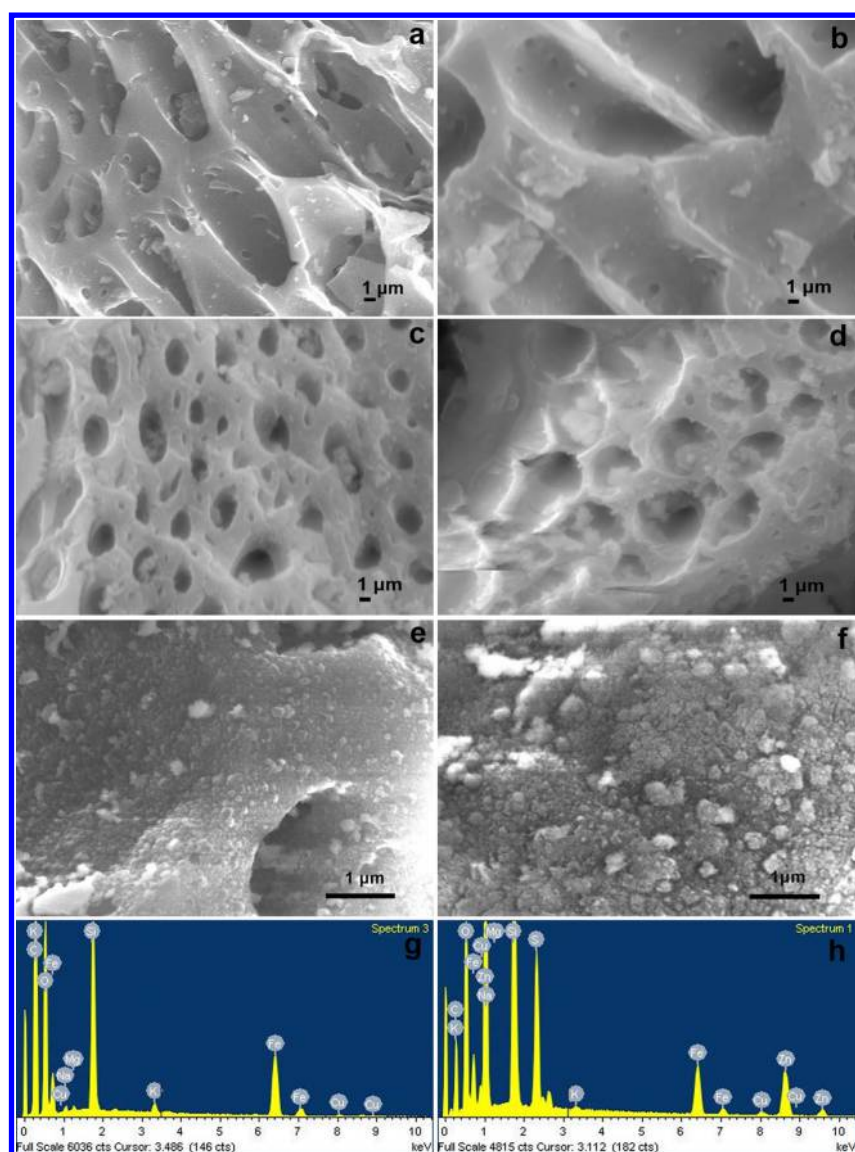


Figure 1. XRD patterns of MB, MB100, MBZ100-0.5, and MBZ100-1.

small angle could be attributed to the amorphous phase of the biochar that was apparent in all the samples. Six other peaks at 30.1°, 35.42°, 43.05°, 53.39°, 56.94°, and 62.52° can be indexed to planes (220), (311), (400), (422), (511), and (440) of magnetite (JCPDS 19-0629). This indicated that prepared  $\text{Fe}_3\text{O}_4$  with the biochar matrix were well crystallized. Additionally, new peaks at 26.92°, 28.51°, 30.54°, 47.54°, 51.78°, and 56.40° were observed in MBZ100-0.5 and MBZ100-1. The positions of these new peaks correspond to the (100), (002), (101), (110), (103), and (112) planes of the standard XRD of wurtzite-2H ZnS (JCPDS 05-0492). Results from the XRD analysis confirmed that magnetic biochar/ZnS composites were prepared successfully.

Details about the morphology of obtained materials are illustrated in the SEM and TEM images (Figures 2 and 3). Figure 2b clearly shows that the surface of MB100 is covered with  $\text{Fe}_3\text{O}_4$  nanoparticles, which were formed with the decomposition of  $\text{Fe}(\text{acac})_3$ . It is totally different from the naked surface of biochar (Figure 2a). After the deposition process of ZnS NCs, it was found that some smaller ZnS NCs embedded in the pores and dispersed on the surface of magnetic biochar (Figure 2c,d). It was obvious that the ZnS layer on magnetic biochar would be much thicker with increasing the deposition time from 0.5 to 1 h (Figure 2e,f). Furthermore, TEM images are in good agreement with the morphology analysis presented in SEM images. First, a good dispersion of  $\text{Fe}_3\text{O}_4$  has been observed (Figure 3a). The high-resolution TEM (HRTEM) image of MB100 shows the sizes are about 7–8 nm (Figure 3a1) which is in agreement with the results calculated by the Scherrer Equation. The clear lattice spacing of 0.25 nm (Figure 3a2) can be assigned to the (311) plane of  $\text{Fe}_3\text{O}_4$ . Second, the coating of ZnS NCs on magnetic biochar is displayed in the TEM images (Figure 3b,c). Consistent with the results calculated by the Scherrer Equation from the strongest diffraction peak (100), the sizes of the ZnS



**Figure 2.** SEM images and EDX results of composites: (a) SEM image of biochar ( $\times 3000$ ), (b) SEM image of MB100 ( $\times 3000$ ), (c) SEM image of MBZ100-0.5 ( $\times 3000$ ), (d) SEM image of MBZ100-1 ( $\times 3000$ ), (e) SEM image of MBZ100-0.5 ( $\times 20,000$ ), and (f) SEM image of MBZ100-1 ( $\times 20,000$ ). EDX results of selected areas of (g) MB100 and (h) MBZ100-1.

NCs in MBZ100-0.5 and MBZ100-1 are about 5 nm. As shown in Figure 3d, two individual nanoparticles show their respective clear lattice fringes with  $d$ -spacings of 0.297 and 0.33 nm, which should be assigned to the (220) plane of  $\text{Fe}_3\text{O}_4$  and (100) plane of ZnS NCs, respectively. The results further reveal that biochar has been decorated with  $\text{Fe}_3\text{O}_4$  nanoparticles and ZnS NCs. The major element composition was analyzed by ICP-AES analysis (Table 1). The determined results showed that there was Zn and Fe in MBZ100-0.5 and MBZ100-1, and the content of Zn in MBZ100-1 was higher than that in MBZ100-0.5. Besides, there was no Zn in MB100. This was further confirmed by EDX spectra. MB100 comprised Fe, C, O, and other trace elements, while MBZ100-1 comprised Zn, S, and the above elements (Figure 2g,h).

Magnetic properties of composite materials are visually depicted in Figure 4. All the samples exhibited superparamagnetic behavior at room temperature with no coercivity and remanence. On the basis of the measurement, saturation magnetizations of MB, MB100, MBZ100-0.5, and MBZ100-1

were 13.6, 14.3, 13.0, and 11.6  $\text{emu g}^{-1}$  at 3 T, respectively. The calcination would result in the improvement of the magnetic properties of the magnetic biochar. Saturation magnetizations of MBZ100-0.5 and MBZ100-1 were lower than MB100, which should be mainly attributable to the dilution effect by ZnS NCs. The magnetic biochar/ZnS composite can be easily dispersed in aqueous solution and form a stable dispersion (inset 1) and be separated from their dispersion by a permanent magnet (inset 2).

**Adsorption Kinetics.** The adsorption kinetics of Pb (II) on magnetic biochar/ZnS composites obtained by contact time are shown in Figure 5. The plots present the amount of Pb (II) adsorbed ( $q_t$ ) onto the sorbents versus contact time. It is noteworthy that the adsorption was rapid during the first 60 min, and the equilibrium was then reached within 200 min when MBZ100-0.5 was added. However, the equilibrium time was comparatively longer after using MBZ100-1, which took 720 min. The results indicated that different sample preparation

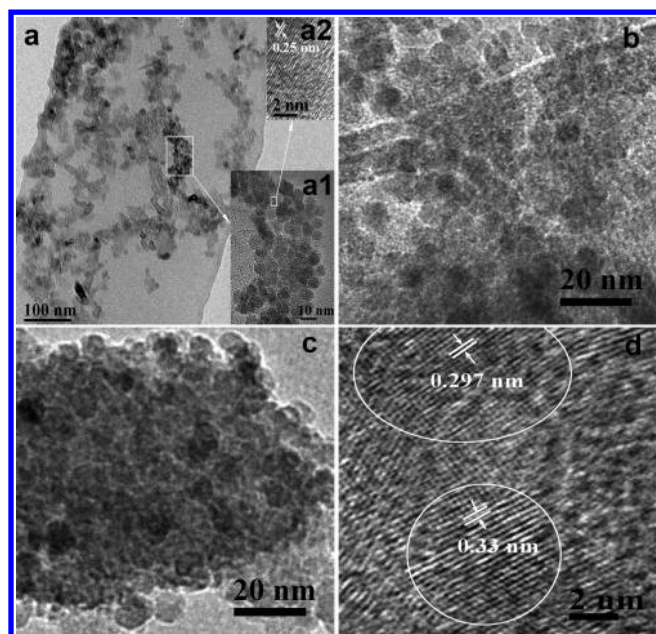


**Figure 3.** TEM images of composites: (a) TEM images of MB100 (insets a1 and a2 are the enlarge image and HRTEM image of the selected area, respectively), (b) TEM image of MBZ100-0.5, (c) TEM image of MBZ100-1, and (d) HRTEM image of MBZ100-0.5.

**Table 1.** Weight Percent of Major Components of Composite Materials

sample	Fe	Fe <sub>3</sub> O <sub>4</sub>	Zn	ZnS
MB100	10.93	15.11	NA <sup>a</sup>	NA <sup>a</sup>
MBZ100-0.5	11.85	16.38	5.94	8.85
MBZ100-1	11.73	16.21	11.86	17.67

<sup>a</sup>No Zn or ZnS.

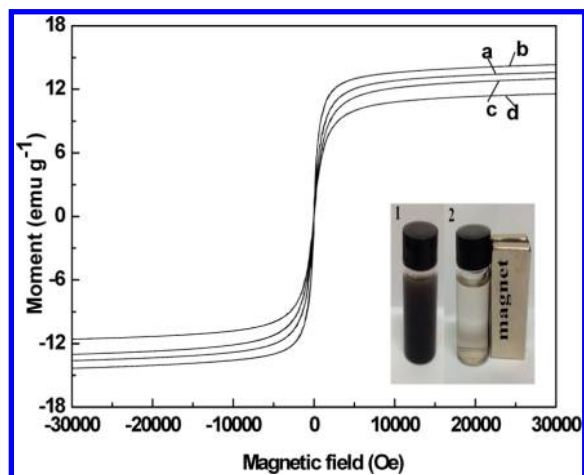


**Figure 4.** Magnetization curves of composites at 300 K: (a) MB, (b) MB100, (c) MBZ100-0.5, and (d) MBZ100-1. Inset is the photograph of dispersion of MBZ100-0.5 in aqueous solution (1) and its response to a magnet (2).

times of sorbents would influence the equilibrium times of adsorption.

In order to investigate the rate mechanism of the adsorption processes, the pseudo-first-order model was applied to analyze the kinetic data. The equation is listed as follows

$$\ln(q_e - q_t) = \ln q_e - k_1 t \quad (2)$$

where  $q_t$  and  $q_e$  refer to the amount of sorption at any time  $t$  and equilibrium ( $\text{mg g}^{-1}$ ), respectively, and  $k_1$  ( $\text{min}^{-1}$ ) is the pseudo-first-order rate constant.<sup>22</sup> The plots of  $\ln(q_e - q_t)$  versus  $t$  show good linearity in the pseudo-first-order model (Figure 5). Values calculated from this model were close to experimental values. The parameters in eq 2 and correlation coefficients  $R^2$  are given in Table 2. As shown in Table 2, correlation coefficients of the pseudo-first-order rate model are 0.9769 for MBZ100-0.5 and 0.9781 for MBZ100-1. Therefore, adsorption kinetics of Pb (II) could be considered as the pseudo-first-order rate mechanism. The rate constant  $k_1$  of pseudo-first-order adsorption was 0.02272  $\text{min}^{-1}$  for MBZ100-0.5 and 0.00952  $\text{min}^{-1}$  for MBZ100-1, respectively. By comparing their rate constants, MBZ100-0.5 showed higher adsorption rate, despite having lower  $q_e$ . It seems that the adsorption rate and  $q_e$  of Pb (II) are closely related to the content of ZnS NCs presented in Table 1. The reaction is faster when the ZnS NCs layer in the MBZ100-0.5 sorbent is thinner, which could be explained by a simple diffusion-controlled reaction scheme, where the reaction time is roughly proportional to the square of the size,<sup>23</sup> and lower  $q_e$  is due to less ZnS NCs coated on MBZ100-0.5. The acceptably high capacity for Pb (II) sorption on MBZ100-1 and fast kinetics for Pb (II) sorption on MBZ100-0.5 exhibit promising potentials for wastewater treatment.

**Adsorption Isotherms.** In addition to adsorption kinetics, adsorption isotherms of Pb (II) onto magnetic biochar/ZnS composites were performed to explore the adsorption mechanism more in-depth. Figure 6 shows the adsorption isotherm of Pb (II) MBZ100-1. As shown in the figure, the adsorption capacity ( $q_e$ ) increased with an increase in equilibrium concentration ( $C_e$ ) and reached a plateau representing the maximum adsorption capacity. Two typical adsorption models, the Langmuir and Freundlich models, were used to simulate the sorption isotherms of Pb (II) onto MBZ100-1.

A basic assumption of the Langmuir model is that the adsorption takes place at specific homogeneous adsorption sites on the sorbent surface with equivalent sorption energy but without mutual interactions between adsorbed molecules.<sup>24,25</sup> The linear version of the Langmuir model based on this assumption can be described as<sup>26</sup>

$$\frac{C_e}{q_e} = \frac{C_e}{q_m} + \frac{1}{q_m K_L} \quad (3)$$

where  $q_e$  is the adsorption amount of Pb (II) on sorbent ( $\text{mg g}^{-1}$ ),  $C_e$  is the Pb (II) equilibrium concentration in solution ( $\text{mg L}^{-1}$ ), and  $q_m$  and  $K_L$  represent the maximum adsorption capacity of Pb (II) and the energy constant related to the heat of adsorption, respectively. A plot of  $C_e/q_e$  versus  $C_e$  presents a straight line of slope  $1/q_m$  and intercept  $1/q_m K_L$  (Figure 6). The Langmuir constant  $K_L$  calculated from this plot was found to be 0.074  $\text{L mg}^{-1}$ . The Langmuir plot appears to be a good fitting model with a correlation coefficient ( $R^2$ ) of 0.9907.

On the basis of the heterogeneous surface adsorption, the formula of the Freundlich isotherm can be expressed as<sup>26</sup>

$$\log q_e = \log K_F + \frac{1}{n} \log C_e \quad (4)$$

where  $q_e$  is the adsorption amount of Pb (II) on sorbent ( $\text{mg g}^{-1}$ ),  $C_e$  is the equilibrium concentration of Pb (II) in solution

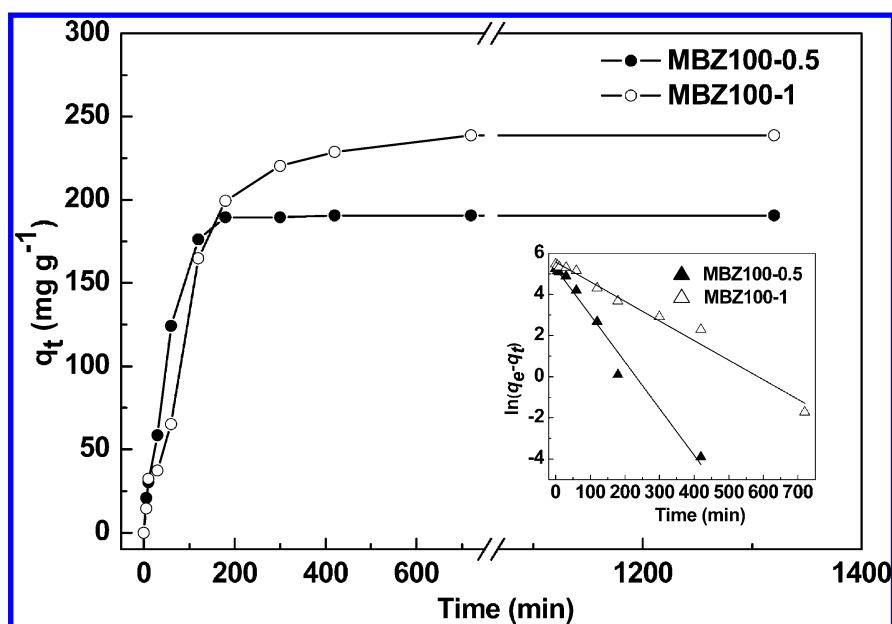


**Figure 5.** Adsorption kinetics of Pb (II) on magnetic biochar/ZnS composites. Inset is fitting of the pseudo-first-order model. Symbols are experimental data. Solid lines represent the fitted curves. Experiment conditions: initial concentration  $100 \text{ mg L}^{-1}$  (50 mL), sorbent 20 mg, pH 6, temperature  $25 \text{ }^\circ\text{C}$ , and contact time 22 h.

**Table 2. Parameters Associated with Pseudo-First-Order Model for Adsorption of Pb (II)**

sorbent	$q_e$ ( $\text{mg g}^{-1}$ )	$k_1$ ( $\text{min}^{-1}$ )	$R^2$
MBZ100-0.5	193.8	0.02272	0.9769
MBZ100-1	262.4	0.00952	0.9781

( $\text{mg L}^{-1}$ ),  $K_F$  is the Freundlich adsorption capacity, and  $1/n$  refers to the Freundlich adsorption intensity parameter. The Freundlich parameters were calculated by the plot of  $\log q_e$  versus  $\log C_e$  (Figure 6). The Freundlich adsorption intensity parameter  $1/n$  was 0.373.  $K_F$  was only  $50.39 \text{ mg g}^{-1}$ , far lower than the experimental data, and the  $R^2$  value of the Freundlich

model (0.9477) is lower than that of the Langmuir model (0.9907), indicating the adsorption of Pb (II) onto MBZ100-1 is mainly controlled by the Langmuir surface adsorption mechanisms. The Langmuir maximum adsorption capacity ( $q_m$ ) of MBZ100-1 was  $367.65 \text{ mg g}^{-1}$ , which was considerably higher than the removal capacity of magnetic pine bark waste biochar ( $29.699 \text{ mg g}^{-1}$ ),<sup>12</sup> magnetic oak bark biochar ( $30.2 \text{ mg g}^{-1}$ ), and magnetic oak wood biochar ( $10.13 \text{ mg g}^{-1}$ ).<sup>27</sup> It was 10 times higher than that of these reported magnetic biochars. These results indicate that the magnetic biochar/ZnS composite can be used as a highly efficient sorbent to remove Pb (II) in water treatment.

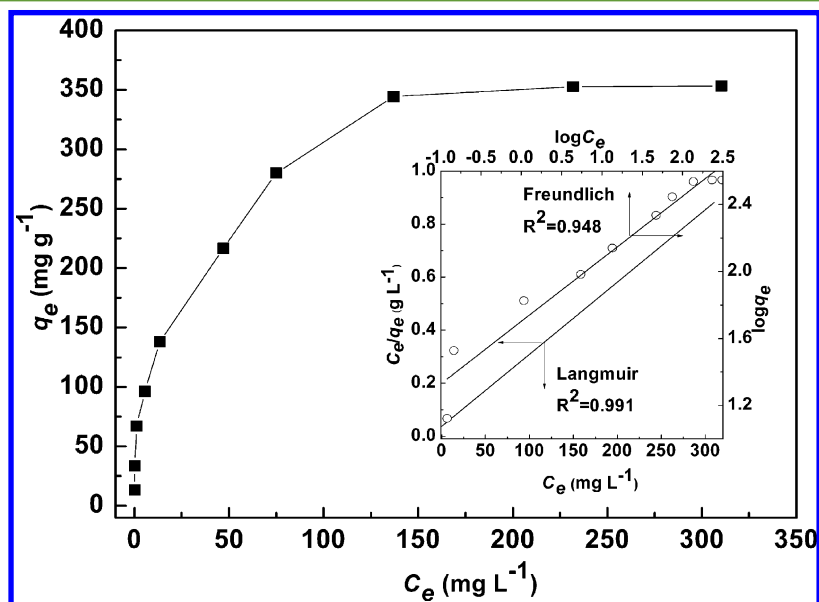


**Figure 6.** Adsorption isotherm of Pb (II) on MBZ100-1. Inset is fitting of Langmuir and Freundlich models. Symbols are experimental data. Solid lines represent the fitted curves. Experiment conditions: initial concentration 20–700  $\text{mg L}^{-1}$  (50 mL), sorbent 60 mg, pH 6, temperature  $25 \text{ }^\circ\text{C}$ , and contact time 24 h.

**Effect of Solution pH and Contact Time.** The effect of solution pH and contact time on Pb (II) adsorption was investigated in an initial pH ranging from 2.0 to 6.0 during 22 h. The adsorption experiment could not be carried out at pH higher than 6 due to the possibility of hydroxide precipitation in Pb (II) solution.<sup>28</sup> The removal efficiency of Pb (II) was due to contact time and was pH dependent (Figure 7). The

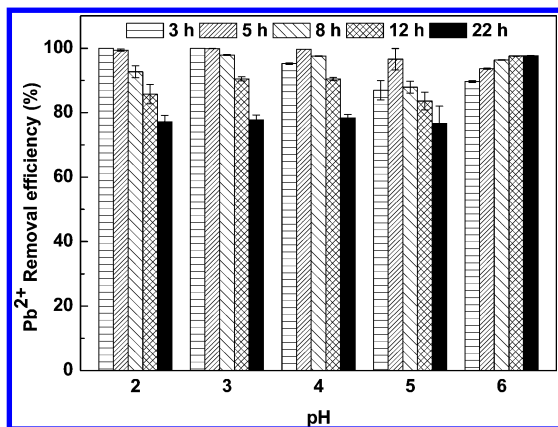


**Figure 7.** Removal efficiency of Pb (II) by MBZ100-1 at different pH values. Experiment conditions: initial concentration 100 mg L<sup>-1</sup> (50 mL), sorbent 20 mg, pH 2–6, temperature 25 °C, and contact time 22 h.

removal efficiency was higher than 97% at pH values 2–5 within 5 h contact time. At pH 2 and 3, the highest removal efficiency occurred at contact time 3 h, but the removal efficiency decreased gradually with a further increase in contact time. At pH 4 and 5, the highest removal efficiency occurred at contact time 5 h. Similarly, the removal efficiency also decreased with increasing contact time beyond 5 h. The main reason is probably that Pb (II) fixed on MBZ100-1 would dissolve at acidic pH values, and the desorption rate was faster with pH values decreasing. However, the desorption phenomenon did not happen at pH 6 (Figure 7). About 97.57% of lead was almost removed and was significantly absorbed at a contact time of 12 h. Therefore, Pb (II) adsorption by magnetic biochar/ZnS composites can be conducted at solution pH 6.

**Removal Efficiency of Magnetic Biochar/ZnS Composite toward Pb (II).** The removal efficiency of the magnetic biochar/ZnS composite (MBZ100-1) at pH 6 is shown in Figure 8, and the removal efficiency of biochar and MB100 was also investigated. In the condition of exceeding the saturation adsorption capacity of MBZ100-1, its removal efficiency was still significantly higher than that of biochar and MB100 at each contact time 7, 18, and 24 h. The removal efficiencies of biochar, MB100, and MBZ100-1 are 8.43%, 4.19%, and 64.50%, respectively. These results suggest that modification of magnetic biochar by adding ZnS NCs can greatly improve the removal efficiency.

Figure 8 also shows the treatment capacity of the magnetic biochar/ZnS composite on Pb (II) in water by changing the dose of the composite. The dose was approximately 0.94 g of sorbent/L of Pb (II) solution volume with an initial Pb (II) concentration of about 60 mg L<sup>-1</sup>. Such efficient Pb (II) adsorption led to a final concentration lower than 1 mg L<sup>-1</sup>, which clearly reached the national wastewater standard stipulated in the Integrated Wastewater Discharge Standard.<sup>29</sup> In the electroplating point source category regulated by U.S.

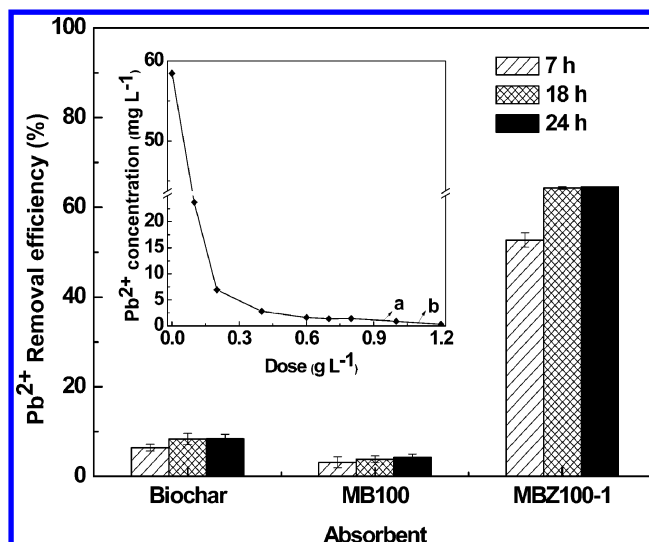


**Figure 8.** Removal efficiency of Pb (II) by three sorbents (biochar, MB100, and MBZ100-1) at 7, 18, and 24 h. Experiment conditions: initial concentration 100 mg L<sup>-1</sup> (50 mL), sorbent 10 mg, pH 6, and temperature 25 °C. Inset is the treatment capacity of MBZ100-1 for the Pb (II) solution. Experiment conditions: initial concentration 60 mg L<sup>-1</sup>, sample dose 0.1–1.2 g of sorbent/L of Pb (II) solution volume, pH 6, temperature 25 °C, and contact time 22 h. Panels a and b represent the waste discharge standard regulated by GB 8978-1996 and the EPA, respectively.

Environmental Protection Agency (EPA),<sup>30</sup> the maximum (any 1 day) for plant discharging is recommended as 0.6 mg L<sup>-1</sup>, so the dose would increase to about 1.1 g of sorbent/L of Pb (II) solution volume. Feng<sup>31</sup> demonstrated that the dose of Pb (II) removal was 5 g of iron slag/L of acid mine drainage with a Pb (II) initial concentration of 4.696 mg L<sup>-1</sup>. The adsorption led to a concentration lower than 1 mg L<sup>-1</sup>. Perić<sup>32</sup> reported the value was 10 g of zeolite/L of Pb (II) solution. The adsorption led to a concentration of 2.5 mg L<sup>-1</sup> from the initial Pb (II) concentration of 113.96 mg L<sup>-1</sup>. In this study, the dose is much lower than these reported values, suggesting that the magnetic biochar/ZnS composite is a preferred adsorbent for remediation of lead-contaminated water.

**Thermodynamics Study.** The thermodynamic parameters, Gibbs free energy ( $\Delta G^0$ ), enthalpy change ( $\Delta H^0$ ), and entropy change ( $\Delta S^0$ ) are useful in defining whether sorption is endothermic or exothermic.<sup>33</sup> Gibbs free energy ( $\Delta G^0$ ) was calculated by following equations<sup>34</sup>

$$K_0 = \frac{a_s}{a_e} = \frac{v_s C_s}{v_e C_e} \quad (5)$$

$$\Delta G^0 = -RT \ln K_0 \quad (6)$$

where  $a_s$  is the activity of adsorbed Pb (II),  $a_e$  is the activity of Pb (II) in solution at equilibrium,  $v_s$  and  $v_e$  are the activity coefficients of adsorbed Pb (II) and Pb (II) in solution at equilibrium, respectively,  $C_s$  is the amount of Pb (II) adsorbed by MBZ100-1 (mmol g<sup>-1</sup>), and  $C_e$  is the concentration of Pb (II) in solution at equilibrium (mmol mL<sup>-1</sup>).  $K_0$  can be obtained by plotting  $\ln(C_s/C_e)$  versus  $C_s$  (Figure 9) and extrapolating  $C_s$  to zero, as the Pb (II) concentration in solution decreases and approaches zero.<sup>34</sup>  $R$  is the gas constant (8.314 J mol<sup>-1</sup> K<sup>-1</sup>), and  $T$  is the absolute temperature in Kelvin.

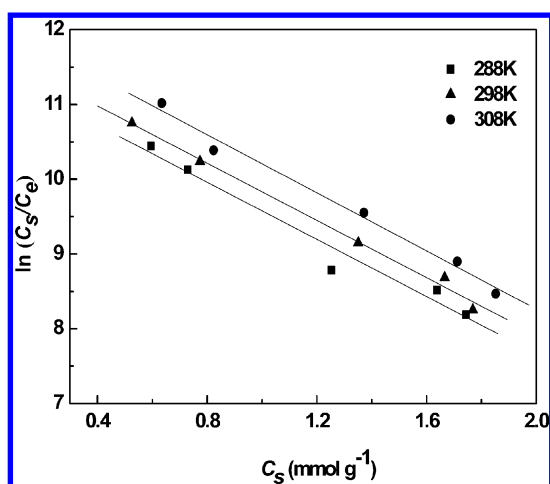


**Figure 9.** Plots of  $\ln(C_s/C_e)$  vs  $C_s$  at 288, 298, and 308 K. Experiment conditions: initial concentration 75–300 mg L<sup>-1</sup> (50 mL), sorbent 30 mg, pH 6, and contact time 24 h.

Enthalpy change ( $\Delta H^\circ$ ) and entropy change ( $\Delta S^\circ$ ) were estimated according to<sup>34,35</sup>

$$\Delta G^\circ = \Delta H^\circ - T\Delta S^\circ \quad (7)$$

$$\ln K_0 = \frac{\Delta S^\circ}{R} - \frac{\Delta H^\circ}{RT} \quad (8)$$

$\Delta H^\circ$  and  $\Delta S^\circ$  were obtained from the slope ( $\Delta H^\circ/R$ ) and intercept ( $\Delta S^\circ/R$ ) of the  $\ln K_0$  versus  $1/T$  plot. Adsorption studies were carried out at three temperatures of 288, 298, and 308 K. The calculated thermodynamic parameters are given in Table 3. The negative value of  $\Delta G^\circ$  implies the feasibility and

**Table 3.** Thermodynamic Parameters for Adsorption of Pb (II) on MBZ100-1

T (K)	$K_0$	$\Delta G^\circ$ (kJ mol <sup>-1</sup> )	$\Delta H^\circ$ (kJ mol <sup>-1</sup> )	$\Delta S^\circ$ (J mol <sup>-1</sup> ·K <sup>-1</sup> )
288	11.49	-5.85		
298	11.75	-6.10	2.05	27.41
308	12.15	-6.39		

spontaneous nature of this reaction, and the values, with raising temperature, are more negative, which indicates that the reaction is more favored and getting relatively easier at higher temperatures. The positive value of  $\Delta H^\circ$  reveals the interaction is an endothermic process. The positive value of  $\Delta S^\circ$  indicates an increase in disorder and randomness at the solid and solution interface of lead with MBZ100-1 during the adsorption process.<sup>36</sup>

## CONCLUSIONS

Novel magnetic biochar/ZnS composites were prepared by introducing ZnS NCs to magnetic biochar. The sorbents can significantly improve the adsorption capacity of biochar for Pb (II). MBZ100-1 exhibited high adsorption capacity (367.65 mg g<sup>-1</sup>). The adsorption of Pb (II) was of an endothermic nature and was a spontaneous process. The substantially lower cost of the material and its economic feasibility and magnetic separation, as well as efficient adsorption capacity, become the main advantages of this new composite. These preliminary results demonstrate that magnetic biochar/ZnS will have a great potential for lead removal in water.

## AUTHOR INFORMATION

### Corresponding Authors

\*(L.L.) E-mail: liangli117@sjtu.edu.cn. Tel.: +86 21 54745591.

\*(G.S.) E-mail: gqsh@sjtu.edu.cn. Tel.: +86 21 34206925.

### Notes

The authors declare no competing financial interest.

## ACKNOWLEDGMENTS

This study was supported by the National Natural Science Foundation of China (NSFC 21271179), National Natural Science Foundation of China (21477075), Program for New Century Excellent Talents (NCET-13-0364), and National High Technology Research and Development Program (2012AA062504).

## ABBREVIATIONS

NCs, nanocrystals; QDs, quantum dots; Fe(acac)<sub>3</sub>, Ferric acetylacetonate; EG, ethylene glycol; TREG, triethylene glycol; MB, magnetic biochar

## REFERENCES

- (1) Naeem, A.; Saddique, M. T.; Mustafa, S.; Kim, Y.; Dilara, B. Cation exchange removal of Pb from aqueous solution by sorption onto NiO. *J. Hazard. Mater.* **2009**, *168*, 364–368.
- (2) Ayoub, A.; Venditti, R. A.; Pawlak, J. J.; Salam, A.; Hubbe, M. A. Novel hemicellulose–chitosan biosorbent for water desalination and heavy metal removal. *ACS Sustainable Chem. Eng.* **2013**, *1*, 1102–1109.
- (3) Kavak, D. Removal of lead from aqueous solutions by precipitation: Statistical analysis and modeling. *Desalin. Water Treat.* **2013**, *51*, 1720–1726.
- (4) Soylak, M.; Cay, R. S. Separation/preconcentration of silver (I) and lead (II) in environmental samples on cellulose nitrate membrane filter prior to their flame atomic absorption spectrometric determinations. *J. Hazard. Mater.* **2007**, *146*, 142–147.
- (5) Gollavelli, G.; Chang, C. C.; Ling, Y. C. Facile synthesis of smart magnetic graphene for safe drinking water: heavy metal removal and disinfection control. *ACS Sustainable Chem. Eng.* **2013**, *1*, 462–472.
- (6) Feng, J.; Yang, Z. H.; Zeng, G. M.; Huang, J.; Xu, H. Y.; Zhang, Y. Y.; Wei, S. M.; Wang, L. The adsorption behavior and mechanism investigation of Pb (II) removal by flocculation using microbial flocculant GA1. *Bioresour. Technol.* **2013**, *148*, 414–421.
- (7) Perić, J.; Trgo, M.; Medvidović, N. V. Removal of zinc, copper and lead by natural zeolite—A comparison of adsorption isotherms. *Water Res.* **2004**, *38*, 1893–1899.
- (8) Lehmann, J.; Joseph, S. *Biochar for Environmental Management: Science and technology*; Earthscan: London, 2009.
- (9) Mohan, D.; Sarswat, A.; Ok, Y. S.; Pittman, C. U., Jr. Organic and inorganic contaminants removal from water with biochar, a renewable, low cost and sustainable adsorbent—A critical review. *Bioresour. Technol.* **2014**, *160*, 191–202.
- (10) Chen, B. L.; Chen, Z. M.; Lv, S. F. A novel magnetic biochar efficiently sorbs organic pollutants and phosphate. *Bioresour. Technol.* **2011**, *102*, 716–723.
- (11) Zhang, M.; Gao, B.; Varnosfaderani, S.; Hebard, A.; Yao, Y.; Inyang, M. Preparation and characterization of a novel magnetic biochar for arsenic removal. *Bioresour. Technol.* **2013**, *130*, 457–462.
- (12) Reddy, D. H. K.; Lee, S. M. Magnetic biochar composite: Facile synthesis, characterization, and application for heavy metal removal. *Colloids Surf., A* **2014**, *454*, 96–103.
- (13) Qu, X. L.; Alvarez, P. J. J.; Li, Q. L. Applications of nanotechnology in water and wastewater treatment. *Water Res.* **2013**, *47*, 3931–3946.
- (14) Li, Q. L.; Mahendra, S.; Lyon, D. Y.; Brunet, L.; Liga, M. V.; Li, D.; Alvarez, P. J. J. Antimicrobial nanomaterials for water disinfection and microbial control: Potential applications and implications. *Water Res.* **2008**, *42*, 4591–4602.

- (15) Ghasemzadeh, G.; Momenpour, M.; Omid, F.; Hosseini, M. R.; Ahani, M.; Barzegari, A. Applications of nanomaterials in water treatment and environmental remediation. *Front. Environ. Sci. Eng.* **2014**, *8*, 471–482.
- (16) Kusic, H.; Leszczynska, D.; Koprivanac, N.; Peternel, I. Role of quantum dots nanoparticles in the chemical treatment of colored wastewater: Catalysts or additional pollutants. *J. Environ. Sci.* **2011**, *23*, 1479–1485.
- (17) Alivisatos, A. P. Semiconductor clusters, nanocrystals, and quantum dots. *Science* **1996**, *271*, 933–937.
- (18) Pala, I. R.; Brock, S. L. ZnS nanoparticle gels for remediation of Pb<sup>2+</sup> and Hg<sup>2+</sup> polluted water. *ACS Appl. Mater. Interfaces* **2012**, *4*, 2160–2167.
- (19) Piquette, A.; Cannon, C.; Apblett, A. W. Remediation of arsenic and lead with nanocrystalline zinc sulfide. *Nanotechnol.* **2012**, *23*, 294014.
- (20) Jaiswal, A.; Ghosh, S. S.; Chattopadhyay, A. Quantum dot impregnated-chitosan film for heavy metal ion sensing and removal. *Langmuir* **2012**, *28*, 15687–15696.
- (21) Shang, G. F.; Shen, G. Q.; Liu, L.; Chen, Q.; Xu, Z. W. Kinetics and mechanisms of hydrogen sulfide adsorption by biochars. *Bioresour. Technol.* **2013**, *133*, 495–499.
- (22) Lin, S. H.; Juang, R. S. Heavy metal removal from water by sorption using surfactant-modified montmorillonite. *J. Hazard. Mater.* **2002**, *92*, 315–326.
- (23) Huang, D. W.; Niu, C. G.; Ruan, M.; Wang, X. Y.; Zeng, G. M.; Deng, C. H. Highly sensitive strategy for Hg<sup>2+</sup> detection in environmental water samples using long lifetime fluorescence quantum dots and gold nanoparticles. *Environ. Sci. Technol.* **2013**, *47*, 4392–4398.
- (24) Özacar, M.; Şengil, I. A. Adsorption of reactive dyes on calcined alunite from aqueous solutions. *J. Hazard. Mater.* **2003**, *98*, 211–224.
- (25) Li, Y. H.; Du, Q. J.; Wang, X. D.; Zhang, P.; Wang, D. C.; Wang, Z. H.; Xia, Y. Z. Removal of lead from aqueous solution by activated carbon prepared from *Enteromorpha prolifera* by zinc chloride activation. *J. Hazard. Mater.* **2010**, *183*, 583–589.
- (26) Motsa, M. M.; Mamba, B. B.; Thwala, J. M.; Msagati, T. A. M. Preparation, characterization, and application of polypropylene-clinoptilolite composites for the selective adsorption of lead from aqueous media. *J. Colloid Interface Sci.* **2011**, *359*, 210–219.
- (27) Mohan, D.; Kumar, H.; Sarswat, A.; Alexandre-Franco, M.; Pittman, C. U., Jr. Cadmium and lead remediation using magnetic oak wood and oak bark fast pyrolysis biochars. *Chem. Eng. J.* **2014**, *236*, 513–528.
- (28) Hadi, P.; Barford, J.; McKay, G. Toxic heavy metal capture using a novel electronic waste-based material mechanism, modeling and comparison. *Environ. Sci. Technol.* **2013**, *47*, 8248–8255.
- (29) *Integrated Wastewater Discharge Standard*; GB 8978-1996; Beijing Ministry of environmental protection of China: Beijing, 1996.
- (30) Electroplating Point Source Category. *Code of Federal Regulations*, Part 413, Title 40, 1981. <http://www.ecfr.gov/cgi-bin/ECFR?page>.
- (31) Feng, D.; Van Deventer, J. S. J.; Aldrich, C. Removal of pollutants from acid mine wastewater using metallurgical by-product slags. *Sep. Purif. Technol.* **2004**, *40*, 61–67.
- (32) Perić, J.; Trgo, M.; Medvidović, N. V. Removal of zinc, copper, and lead by natural zeolite—A comparison of adsorption isotherms. *Water Res.* **2004**, *38*, 1893–1899.
- (33) Chen, X. C.; Chen, G. C.; Chen, L. G.; Chen, Y. X.; Lehmann, J.; McBride, M. B.; Hay, A. G. Adsorption of copper and zinc by biochars produced from pyrolysis of hardwood and corn straw in aqueous solution. *Bioresour. Technol.* **2011**, *102*, 8877–8884.
- (34) Li, Y. H.; Di, Z. C.; Ding, J.; Wu, D. H.; Luan, Z. K.; Zhu, Y. Q. Adsorption thermodynamic, kinetic and desorption studies of Pb<sup>2+</sup> on carbon nanotubes. *Water Res.* **2005**, *39*, 605–609.
- (35) Liu, Z. G.; Zhang, F. S. Removal of lead from water using biochars prepared from hydrothermal liquefaction of biomass. *J. Hazard. Mater.* **2009**, *167*, 933–939.
- (36) Irani, M.; Amjadi, M.; Mousavian, M. A. Comparative study of lead sorption onto natural perlite, dolomite and diatomite. *Chem. Eng. J.* **2011**, *178*, 317–323.